Highly Efficient Broadband Ambient Energy Harvesting System Enhanced by Meta-Lens for Wirelessly Powering Battery-less IoT Devices

Article in IEEE Internet of Things Journal · October 2023

DOI: [illegible]

[illegible] Wang
Wuhan University of Technology

[illegible] Qiu
Wuhan University of Technology

Lei Wang
Lancaster University

[illegible]
University of Electronic Science and Technology of China

Highly Efficient Broadband Ambient Energy Harvesting System Enhanced by Meta-lens for Wirelessly Powering Battery-less IoT Devices

Yuchao Wang, Shi He, Yongxue Qiu, Ruiyuan Wu, Lei Wang, *Senior Member*, *IEEE*, Ping Lu, *Member*, *IEEE*, Chaoyun Song, *Senior Member*, *IEEE*, Qiang Cheng, *Senior Member*, *IEEE*, and Cheng Zhang, *Member*, *IEEE*

***Abstract*—Existing Internet of Things (IoT) devices face a significant challenge in terms of power consumption due to their limited battery life. Capturing and utilizing ambient radio frequency (RF) energy emerges as a promising solution for powering low-power sensors and electronic devices, given its unique spatial and temporal distributions. However, the low level of ambient RF power severely hampers the rectenna's RF-to-direct current (DC) conversion efficiency, making it incapable of generating sufficient DC power. To address this issue and enhance the conversion efficiency of a broadband rectenna at low environmental power levels, this study introduces a novel technique called the meta-lens assisted technique (MAT). This technique leads to a substantial increase in the rectenna's received RF power by more than 10 dB. As a result, the total conversion efficiency improves by over 30% across a wide frequency band ranging from 2.9 GHz to 3.63 GHz (with a fractional bandwidth of 22.3%), even when the initial RF power received (without the MAT) was as low as -20 dBm, which approaches the real-life ambient RF power level. Notably, the proposed MAT achieves a 40% to 60% efficiency improvement compared to state-of-the-art approaches. These remarkable results demonstrate the promising potential of the MAT rectenna as an alternative for harvesting low-density wireless energy and supporting low-power-required industrial IoT applications.**

***Index Terms*—Broadband rectenna, meta-lens assisted technique, rectifier, RF energy harvesting, Internet of Things (IoT), and Industrial IoT (IIoT).**

I. INTRODUCTION

RECENTLY, the emerging Internet of Things (IoTs) has shown significant growth in wireless communications, environmental monitoring, human-to-machine systems and biomedical health services [1-3], where batteries with a limited life span are commonly used for GPS, active RFID and wireless sensor nodes in generic IoT systems [4-6]. However, these have several maintenance issues such as it needs frequent recharging/replacement and it has limited durability. Therefore, sustainable, eco-friendly, and non-conventional energy sources have become increasingly more crucial. With further advancements in wireless communication technology, radio frequency (RF) sources have also sharply increased [7-12]. Hence, directly adopting RF energy may help eliminate batteries and facilitate self-sustaining devices.

Rectennas have been the subject of research for several decades due to their critical role in RF energy harvesting, particularly in the context of improving RF-to-direct current (RF-DC) conversion efficiency, especially at low-power levels [13-16]. However, when considering the physical characteristics of the diode [17-20], it becomes evident that the intrinsic conversion efficiency of existing rectennas is directly correlated with the input RF power [21-23]. For instance, as documented in [24], high-efficiency 2.45-GHz rectennas achieve an efficiency of 72% at an input power level of 0 dBm, but this efficiency drops to 40% when the input power decreases to -20 dBm. In reality, ambient RF power density typically ranges from -35 to -10 dBm/m2 [25], and the majority of reported rectenna efficiencies in such conditions fall below 50% [26-30]. Consequently, enhancing the RF-DC conversion efficiency of rectennas at low-power levels, such as those found in ambient signals, continues to pose a significant challenge.

Meanwhile, considering the power accumulation benefits, the rectifiable frequency band and effective power spectrum are also crucial factors in harvesting sufficient RF energy, in addition to the conversion efficiency [31-33]. Compared with the multi-band rectenna [34-36], broadband rectennas have better uplink and downlink coverages as it simultaneously operates both bands [37], which, in turn, can have significant advantages in energy accumulation and DC output power generation. Currently, the relative bandwidth of rectennas can be extended to more than 80% [38-40], however, its validation is limited to only high input power levels (>10 dBm).

This work was supported in part by the National Key Research and Development Program of China (2018YFA0701904, 2017YFA0700201, and 2017YFA0700202, 2017YFA0700203), the National Natural Science Foundation of China (62101394, 61722106, 62001338 and 61731010), the Fundamental Research Funds for the Central Universities (WUT: 2021IVA064, 2021IVB029, and 2021III006JC), and the Foundation from the Guangxi Key Laboratory of Optoelectronic Information Processing (GD21203).
(*Corresponding authors: Ruiyuan Wu; Chaoyun Song; Cheng Zhang.*)

Y. Wang and C. Zhang are with Shanghai Institute of Optics and Fine Mechanics, Chinese Academy of Sciences, Shanghai 201800, China (e-mail: yuchao9629@whut.edu.cn; czhang2020@whut.edu.cn).

Y. Wang and Y. Qiu are with Wuhan University of Technology, Wuhan 430070, China (e-mail: yuchao9629@whut.edu.cn; yxqiu1999@whut.edu.cn).

S. He, R. Wu, and Q. Cheng are with the State Key Laboratory of Millimeter Waves, Southeast University, Nanjing 210096, China (e-mail: 2698185976@qq.com; ruiyuanwu@126.com; qiangcheng@seu.edu.cn).

L. Wang is with the School of Engineering and Physical Sciences, Institute of Sensors, Signals and Systems, Heriot-Watt University, EH14 4AS, United Kingdom. (e-mail: wanglei@ieee.org).

P. Lu is with the School of Electronics and Information Engineering, Sichuan University, Chengdu 610064, China (e-mail: pinglu90@scu.edu.cn)

C. Song is with State Key Laboratory of Radio Frequency Heterogeneous Integration, College of Electronics and Information Engineering, Shenzhen University, Shenzhen 518060, China. He is also with the Department of Engineering, King's College London, London, WC2R 2LS, UK (e-mail: chaoyun.song@kcl.ac.uk).

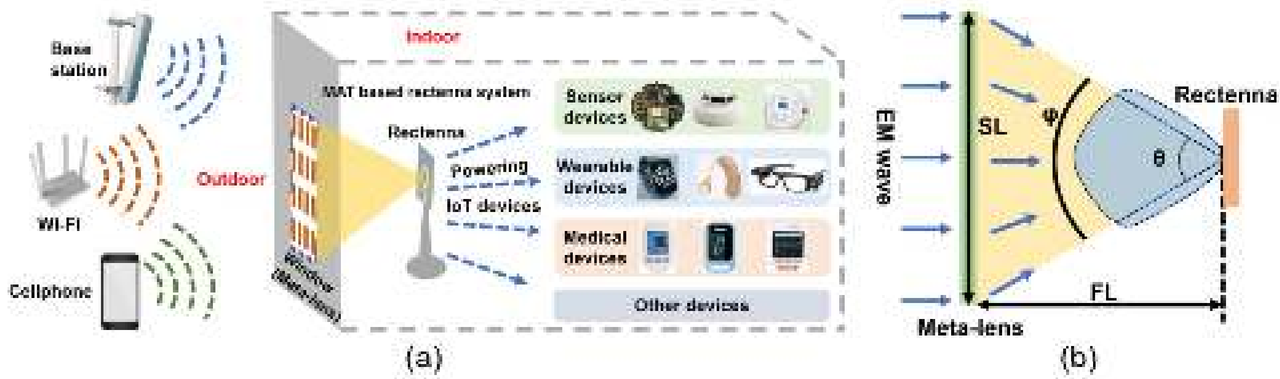

Fig. 1. (a) Illustration of the MAT based rectenna system. For future applications, the meta-lens could be embedded into window or home furniture using specific material (transparent metal) for enhanced energy harvesting for low power IoT devices. (b) Design schematic of the MAT enhanced wireless energy harvesting system.

Meanwhile, the rectenna bandwidth can be hardly expanded in low input power levels, owing to the high Q-factor of the rectifying network, thereby significantly limiting the design of a broadband matching network [41]. Several attempts have been previously made to develop broadband antennas to address this problem. For instance, a novel impedance-matching network with an additional quarter-wavelength short-circuited stub was proposed in [42] to achieve broadband impedance matching. Although the rectifier was capable of operating at ~1.0 GHz – 2.5 GHz with an input power of −10 dBm, the maximum efficiency was only 30%, owing to a large mismatch between the rectifying network and matching network. Consequently, a high-efficiency broadband rectenna was designed in [43] to improve the RF-DC conversion efficiency and reduce physical matching losses by eliminating the matching network. Here, the design enabled the achievement of the conversion efficiency higher than 30% when the input power level was at −15 dBm. However, the impedance bandwidth where $S_{11} < -10$ dB (2.18 GHz – 2.3 GHz (5.3%); 2.4 GHz – 2.6 GHz (8%)) was still narrow, owing to the restricted conjugate matching. Based on these prior studies, either the impedance or conjugate matching technique can only provide a compromise between the conversion efficiency and operation bandwidth. Hence, there is an urgent demand for new techniques to effectively resolve the tradeoffs between bandwidth and efficiency, especially for low power levels < −20 dBm. Notably, using a meta-lens has a potential in addressing this problem based on theoretical demonstrations in [44] that was able to focus the energy on to an antenna.

In this paper, we introduce a novel meta-lens-assisted technique (MAT) designed to enhance the broadband conversion efficiency of rectennas operating at low input powers. The technique achieves this by effectively regulating the RF field distribution around the rectenna, resulting in improved receiving power and enhanced conversion efficiency, as depicted in Fig. 1(a). By strategically focusing input RF waves within a specific area, the MAT enables practical wireless charging capabilities. The design (Fig. 1(b)) aims to maximize the capture of input RF energy using the fundamental design principle of optimizing field of view (FOV: φ) of the meta-lens to be approximately equal to the 3-dB beam width (θ) of the receiving antenna, in which this was considered as the basis of the MAT-enhanced system. Furthermore, the rectifier was optimized in synchronization with the working bandwidth and real input power level, both with and without MAT.

The rest of this paper is structured as follows: Section II presents the proposed broadband rectifier, in which it provides a discussion on achieving an efficiency of over 40% within the frequency range of 2.96 GHz to 3.62 GHz, with an input power of −10 dBm. It also provides a discussion on achieving an efficiency of 18% at an ultralow input power of −20 dBm. Section III details the design of the broadband receiving antenna and its corresponding meta-lenses, in which it discusses how the receiving power of the antenna was enhanced by more than 10 dB. Finally, in Section IV, we rigorously quantify and discuss the impact of the meta-lens-assisted technique on receiving power and conversion efficiency.

II. Broadband Rectifier Design

To achieve the RF-DC conversion system shown in Fig. 1, a broadband rectifier should first be designed to determine the operating band for the subsequent receiving antenna and meta-lens design. Generally, the rectifier consists of an impedance-matching network for maximum power delivery, a rectifying element for received energy conversion, and a DC-pass filter to smooth the output voltage and load [45-46]. To date, various types of rectifiers such as the single series diode rectifier [47], single shunt diode rectifier [48], voltage doubler rectifier [49], and full-wave Greinacher rectifier [50], have been investigated to convert the harvested RF power to DC power. The traditional single-series diode rectifier cannot convert energy efficiently, and the voltage doubler rectifier and Greinacher rectifier have complicated structures that cause a large energy loss at the diodes [50]. Hence, a single-shunt diode rectifier was chosen to achieve high conversion efficiency within a broad operation band.

In this section, matching and rectifying networks were designed independently to explore their contributions to the

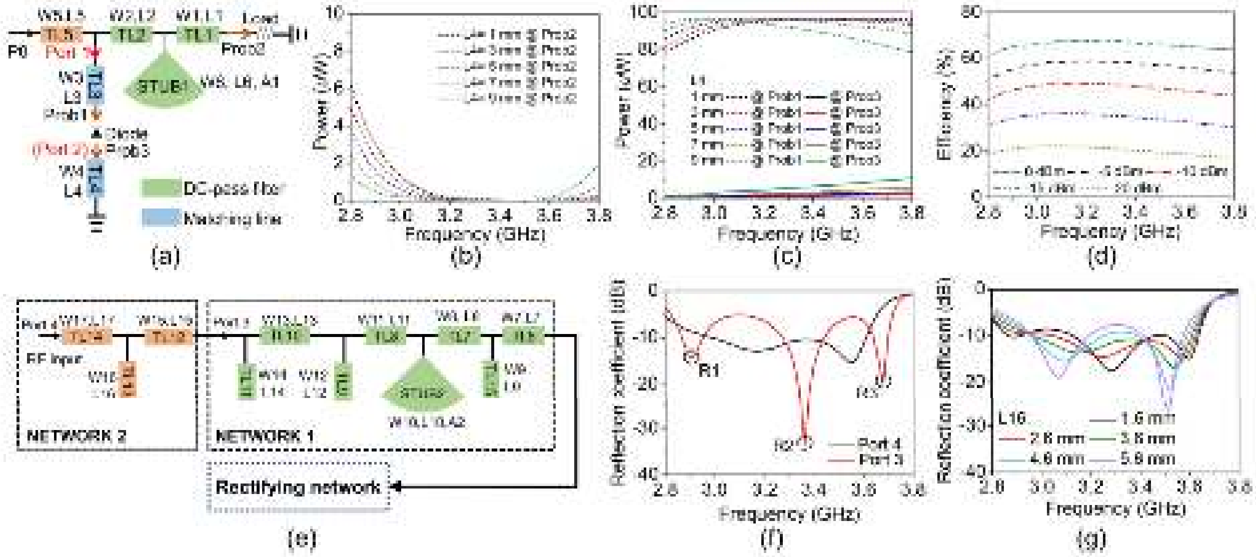

Fig. 2. (a) Topology of the proposed rectifying network. Simulated power of Prob2 (b) and Prob1/Prob3 (c) of the proposed rectifying network with different values of L4. (d) Simulated RF-DC conversion efficiency of the proposed rectifying network at different input power levels for a load resistance of 1500 Ω. (e) Topology of the proposed matching network. (f) Simulated reflection coefficient of the Port 3 and Port 4 as a function of frequency. (g) Simulated reflection coefficient of the Port 4 as a function of frequency with different value of L16.

TABLE I
GEOMETRIC PARAMETERS OF THE PROPOSED RECTIFIER

Parameter	Value (mm)	Parameter	Value (mm)	Parameter	Value (mm)
L1	8.3	L2	0.8	L3	6.2
L4	5.0	L5	3.5	L6	3.5
L7	5.0	L8	12.7	L9	7.7
L10	8.4	L11	5.4	L12	14.0
L13	2.6	L14	2.6	L15	0.5
L16	3.2	L17	5.0	W1	2.2
W2	2.2	W3	0.5	W4	2.5
W5	4.5	W6	2.2	W7	4.5
W8	4.5	W9	4.5	W10	4.5
W11	2.5	W12	0.2	W13	3.5
W14	2.2	W15	3.2	W16	4.0
W17	2.2	A1	70.0	A2	70.0

bandwidth extension and RF-DC conversion efficiency. Firstly, a broadband rectifying network was proposed to efficiently convert the RF energy into DC power at the 3.0 GHz – 3.6 GHz (covering 5G band), which consists of a DC-pass filter, matching lines, a diode, and a load, as shown in Fig. 2(a). The Schottky diode SMS7630 was selected as the rectifier diode, owing to its low bias voltage requirements at low power input levels and low losses (forward bias voltage: 60–120 mV at 0.1 mA) [51]. Based on the selected diode, a broadband DC-pass filter with optimized transmission lines (TL1 and TL2) and one radial stub (STUB1) was initially designed to successfully convert the input RF energy into DC power and ensure that most of the RF energy could flow into Port 1 (Fig. 2(a)), rather than onto the load by adjusting the input impedance.

Additionally, not all the RF energy flowing into Port 1 is efficiently converted into DC power, owing to the leakage of RF energy into the ground through the diode. Therefore, a matching transmission line (TL4) with the length of L4 was designed to adjust the input impedance of the Port 2 to prevent the leakage of RF energy. To further investigate the effects of the TL4 length on the RF energy distribution, three power probes (Prob1, Prob2, and Prob3) were used to detect the specific RF power, in which the input power was fixed to 100 nW, as shown in Fig. 2(a). Meanwhile, Fig. 2(b) shows the power detected by Prob2 having different values of L4, in which less significant changes correspond to higher isolation performance for the proposed DC-pass filter. Furthermore, the power detected by Prob1 and Prob3 is also revealed in Fig. 2(c). The curves for power detected by Prob1 exhibited fluctuations as the frequency enhances, whereas its counterparts, which were the associated leakage energy detected by Prob3, showed an increasing trend. Accounting for these factors, the value of the L4 was set to 5 mm to simultaneously achieve the maximum operating bandwidth and conversion efficiency.

Although the RF power path was investigated to verify the performance of the DC-pass filter and matching line, the RF-DC conversion efficiency should also be determined as efficiency is the main criterion of the rectifying network. Fig. 2(d) shows the simulated RF-DC conversion efficiency against the frequency with different input power levels. It is apparent that the designed rectifying network was able to achieve stable and relatively high conversion efficiency during the working band even at different input powers (e.g., −20 dBm, −15 dBm, −10 dBm, −5 dBm), thereby exhibiting high broadband performance. To obtain a complete broadband rectifier, designing a broadband matching network that can transfer the input impedance of the rectifying network to the standard 50 Ω is necessary, in which a five-stub tuning optimization method (TL9, TL11, TL13, TL15, and STUB2) was used. NETWORK 1 as a part of the matching network was first designed to

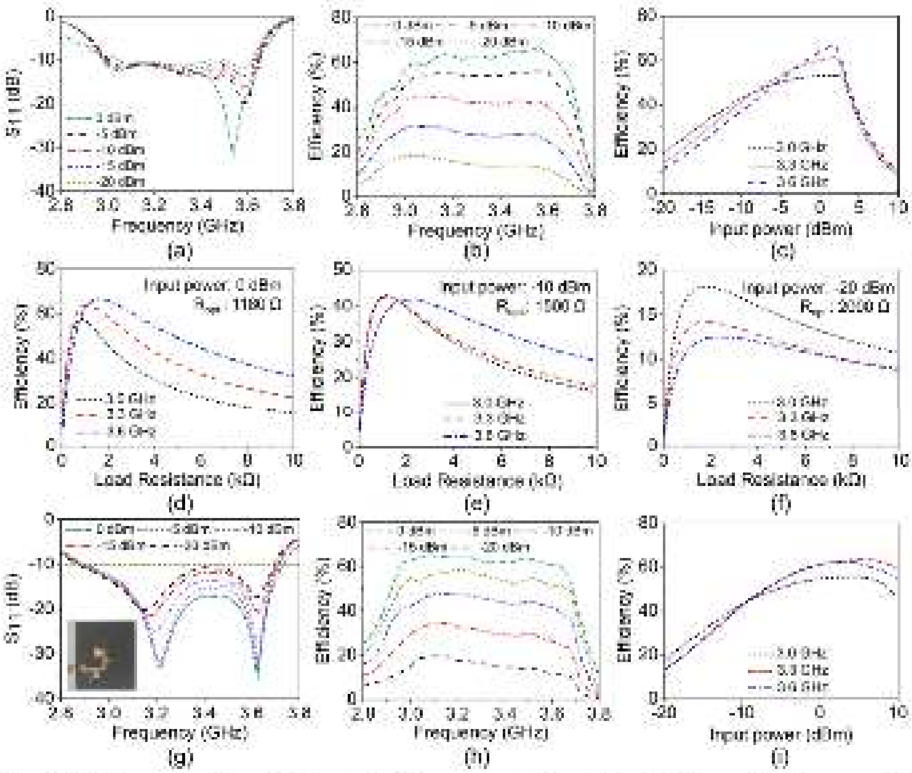

Fig. 3. Simulated S_{11} (a) and RF-DC conversion efficiency (b) of the proposed rectifier at different input power level. (c) Simulated RF-DC conversion efficiency of the proposed rectifier versus input power level at three frequencies. Simulated RF-DC conversion efficiency of the proposed rectifier versus load resistance at three frequencies as the input power is 0 dBm (d), −10 dBm (e), and −20 dBm (f). Measured reflection coefficient (g) and RF-DC conversion efficiency (h) of the proposed rectifier at different input power level. (i) Measured RF-DC conversion efficiency of the proposed rectifier versus input power level at three frequencies for a load resistance of 1500 Ω.

generate several resonances that can cover the operational bandwidth. Three low-reflection peaks were observed in Fig. 2(f) (red line) through optimization, which indicates the presence of the required resonances. However, the reflection coefficient between these resonances showed significant decays, owing to considerable separations, and the design criteria requiring a reflection coefficient in the operation band of below −10 dB have not been met.

To address this, another network called NETWORK 2 (Fig. 2(e)) was introduced, in which its inclusion in the design improved the total reflection coefficient to below −10 dB from 3.0 GHz to 3.6 GHz (Fig. 2(f)). An analysis of the length (L16) of TL13 (Fig. 2(g)) revealed that as L16 increased, the first resonance (R1) gradually shifted to a higher frequency, in which it also integrated with the second resonance (R2). Simultaneously, the R2 and third resonance (R3) moved in opposite directions. Generally, it was observed that the combined effect of these shifts significantly enhanced the broadband performance of the matching network.

The optimal dimensions of the transmission lines and stubs in the entire rectifier are listed in Table I. The rectifier, including the rectifying and matching networks, was simulated using the Advanced Design System (ADS) with the aid of a harmonic-balance (HB) simulator and nonlinear SPICE model of the rectifying diode. The simulated S_{11} is a function of the frequency at different input power levels, as shown in Fig. 3(a). Here, the S_{11} was less than −10 dB at the 3.0 GHz ~ 3.6 GHz as the input power varied from 0 dBm to −20 dBm, showing that majority of the RF power inputted into the rectifier flows into the rectifying network, which is then converted to DC power. As evident from our rectifier design, we have considered the antenna as a fixed 50-Ω load. This simplification represents an approximation of the load imposed by the antenna on the rectifier and is a commonly adopted approach in rectenna design [11, 14, 20, 25, 28, 34, 35]. To further enhance the rectenna's performance, a potential avenue for future work is the co-design of the rectifier and antenna using conjugate matching [3, 13].

Then to analyze the overall RF-DC conversion efficiency of the rectifier, the RF-DC conversion efficiency was simulated as a function of the frequency at different input power levels, as shown in Fig. 3(b). The proposed broadband rectifier showed high conversion efficiency, whereas the efficiency can reach more than 40% at the band of 2.98 GHz ~ 3.62 GHz when the input power was fixed at −10 dBm, which was slightly lower than that of the proposed rectifying network at similar input power levels, owing to the loss of the matching network. Based on the input power level of the corresponding input power of the rectifier performance, the RF-DC power-dependent conversion efficiency is depicted in Fig. 3(c). Here, three different frequencies were used based on the RF-DC conversion efficiencies of the rectifier: 42% @ 3.0 GHz, 42% @ 3.3 GHz, and 40% @ 3.6 GHz at the input power level of −10 dBm. The RF-DC conversion efficiency was observed to gradually

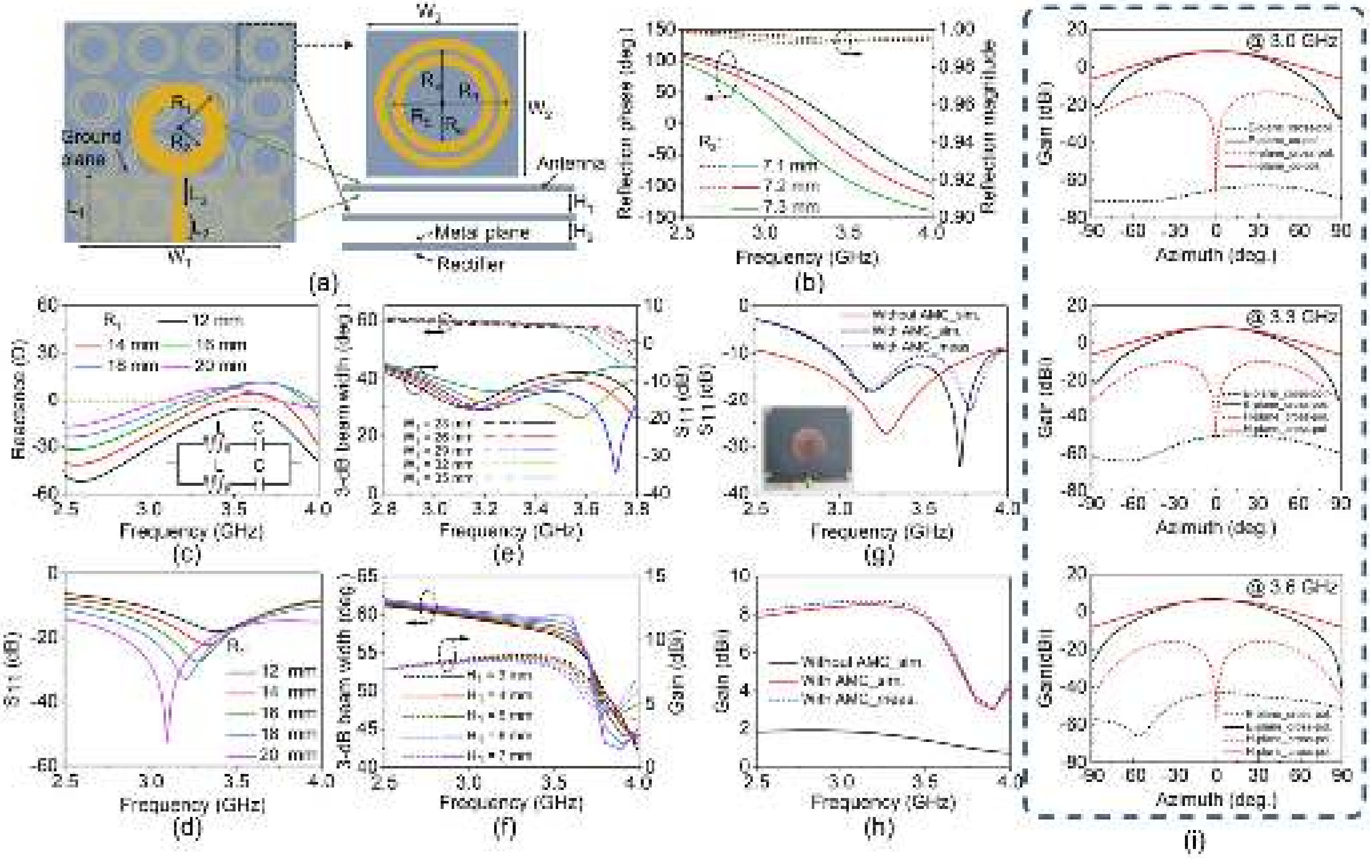

Fig. 4. (a) Geometry of the proposed antenna with AMC. (b) Simulated reflection phase and S_{11} of the AMC as a function of frequency with different values of R_3. Simulated reactance (c) and S_{11} (d) of the antenna without AMC as a function of frequency with different values of R_1. (e) Simulated 3-dB beam width (E-plane) and S_{11} of the proposed antenna with different values of W_1. (f) Simulated 3-dB beam width (E-plane) and gain of the proposed antenna with different values of H_1. Simulated and measured S_{11} (g) and gain (h) of the proposed antenna. (i) Simulated cross and co-polarization level for the proposed antenna at 3.0 GHz, 3.3 GHz, and 3.6 GHz.

increase as a function of the power, owing to the nonlinear ***I-V*** behavior of the rectifier. Notably, this phenomenon occurred only prior to the reverse breakdown of the diode, and once the voltage across the diode exceeds the reverse breakdown voltage, the efficiency of the rectifier dramatically decreases, in which it may be attributed to output DC voltage saturation. In addition, the rectifier remained operational with a maximum efficiency of 19% @ 3.0 GHz at an extremely low input RF power of −20 dBm, indicating an acceptable rectification efficiency at low input power levels. To determine the optimized load value, we analyzed the RF-DC conversion efficiency as a function of the load resistance at various frequencies and input power levels, as illustrated in Figs. 3(d-f). After carefully considering the frequency-dependent RF-DC conversion efficiency and load resistance for different input levels, we selected a load resistance of 1500 Ω as the optimized value.

To verify the proposed design, a prototype was printed on a low-cost F4B substrate with a relative permittivity of 2.2 and a loss tangent of 0.001 for frequencies up to 6.0 GHz, as shown in Fig. 3(g). The measured reflection coefficients S_{11} at the input power levels of 0, −5, −10, −15, and −20 dBm, were then respectively plotted in Fig. 3(g). Notably, the measured −10 dB bandwidth covered the 3.0 GHz – 3.6 GHz band, indicating an acceptable impedance matching of the designed broadband rectifier. In addition, the RF-DC efficiency of the rectifier was evaluated at different input power levels, as shown in Fig. 3(h), in which its counterparts were obtained using the following equation:

$$Efficiency = (I_L^2 \times R) / P_{in} \tag{1}$$

where R is the optimal load resistance of the rectifier (1500 Ω); P_{in} is the input power provided by the signal generator; and I_L is the current across the load resistance. Fig. 3(h) shows that the bandwidth covers 2.96 GHz – 3.62 GHz for efficiency > 40% at −10 dBm input power. Moreover, the matched bandwidth of the proposed design (efficiency > 10%) in relation with the −20 dBm power, was observed to have a range of 2.92–3.68 GHz, which was consistent with the simulated result. The measured RF-DC conversion efficiency is shown in Fig. 3(i) as a function of the input power at three different frequencies. Here, the conversion efficiency was shown to gradually improve from −20 dBm to 0 dBm, which was also consistent with the acceptable matching performance (S_{11} < −10 dB) over the wide input power range shown in Fig. 3(a).

III. Receiving Antenna and Meta-lens Design

To guide the input RF power into the proposed rectifier to the maximum extent, a receiving antenna and a meta-lens were jointly designed to ensure that the FOV [52-55] of the meta-lens was equal to the 3-dB beam width of the receiving antenna,

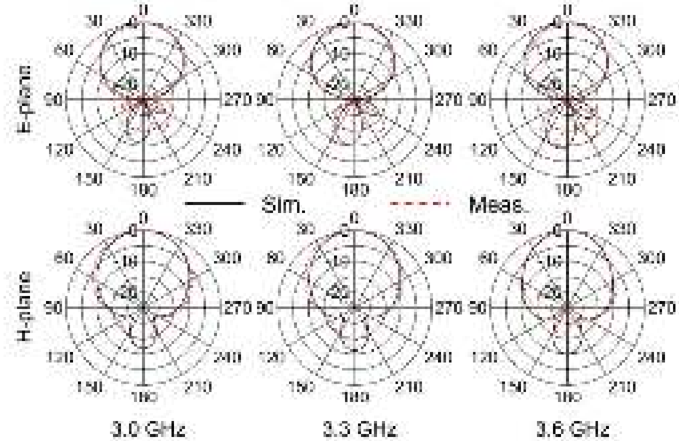

Fig. 5. Simulated and measured 2D radiation patterns of the proposed antenna.

Based on this design principle, the incident waves can be consequently tailored to the primary reception direction of the receiving antenna by the meta-lens; thus, the total efficiency is inferred to be enhanced, owing to the significant increase in the power density around the rectenna. As compared with super-directive antennas, the proposed meta-lens can enhance the antenna radiative field intensity without negatively affecting the 3 dB beam width, and thereby enabling passive amplification by maintaining its original antenna pattern.

4. Receiving Antenna Design

As shown in Fig. 4(a), a broadband monopole antenna integrated with an artificial magnetic conductor (AMC) was designed as the receiving antenna to construct the passive amplification system, owing to its high-gain characteristics (Fig. 4(a)). Meanwhile, because of the monodirectional radiation feature (without backward scattering), the rectifier can be attached to the back of the bottom metallic ground (Fig. 4(a)) to reduce the profile of the total rectenna. The proposed multi-layered broadband high-gain antenna was fabricated on an F4b substrate with a relative permittivity of 2.2 and thickness of 0.762 mm.

Prior to designing the broadband monopole antenna, an AMC structure consisting of two metal rings (Fig. 4(a)) was proposed to operate at 3.0 GHz – 3.6 GHz. The effect of the size of the ring-shaped pattern on the resonant frequency of the AMC was also investigated by conducting simulations to analyze the effect of R_2 on the reflection phase, as shown in Fig. 4(b). The results demonstrated that as R_2 increased, the zero-phase frequency shifted to a lower frequency. Particularly, when R_2 was set to 7.2 mm, the zero-phase frequency was approximately 3.3 GHz. Consequently, the AMC exhibited strong reflection characteristics within the frequency range of 2.75 GHz to 3.83 GHz, in which its corresponding reflection phase was oscillating from −90° to 90° (Fig. 4(b)). Meanwhile, other parameters such as R_3, W_1, and W_2, were optimized based on the operating bandwidth using the commercial software CST Microwave Studio, as shown in Table II. Using the AMC, the impedance bandwidth (Fig. 4(g)) and benefits (Fig. 4(h)) of the designed antenna were expectedly significantly improved. It is worth noting that in the proposed Artificial Magnetic Conductor (AMC) structure, the distance (H_2) between the metal plane and the ring is relatively short. Consequently, the coupling between different modes is relatively small, and the analysis mentioned earlier is specifically performed for the TE_{01} mode. However, when H_2 is increased, the coupling between different modes becomes more significant. This results in multiple zero-phase frequencies appearing in the same wide frequency band, necessitating a multi-mode analysis for multiple frequencies [56-57]. Exploring this direction could be a feasible future step to further consolidate the analysis of this antenna. In this present work, our primary focus has been on evaluating the overall system performance of the wireless energy harvesting system as a whole.

TABLE II
GEOMETRIC PARAMETERS OF THE PROPOSED ANTENNA

Parameter	Value (mm)	Parameter	Value (mm)	Parameter	Value (mm)
R_1	16.0	R_2	5.0	R_3	6.6
R_4	7.8	R_5	5.8	R_6	5.6
L_1	16.0	L_2	5.0	L_3	11.0
W_1	29.0	W_2	18.2	H_1	5.0
H_2	5.0				

Subsequently, a traditional monopole antenna composed of a ring-shaped radiator, a matching line, a feeder line with a characteristic impedance of 50 Ω, and a ground plane, was also designed. Here, the radiator of the antenna was equivalent to a parallel circuit model (inset of Fig. 4(c)), and the resonant frequency of each branch can be expressed as:

$$f = \frac{1}{2\pi\sqrt{LC}} \tag{2}$$

where the equivalent inductance L can be modified by changing the current path length of the radiator; and C is the equivalent capacitance. As the length of the current path increased from the increasing radius R_1 of the radiator, the resonance point shifted to a higher frequency range (Fig. 4(c)). Upon R_1 reaching 16 mm, the antenna achieves an optimal matching performance at a central frequency of 3.3 GHz. Furthermore, this configuration effectively covered the operating band from 3.0 GHz to 3.6 GHz (Fig. 4(d)).

The relative positions of the components are shown in Fig. 4(a). Considering the fixed relative location between the receiving antenna and designed meta-lens, the 3-dB beam width of the proposed antenna was inferred to be stable within the working band. Thus, the width (W_1) of the ground plane was studied in Fig. 4(e), in which it showed that as W_1 increased, the 3-dB beam width of the E-plane sharply decreased at high frequencies. However, the opposite trend showed by W_1 resulted in a deterioration of the impedance bandwidth. Therefore, as the target band was 3.0 GHz – 3.6 GHz, 29 mm was chosen as the optimal value for W_1. In addition, the distance (H_1) between the antenna and AMC mainly affected the surface wave propagation, thereby resulting in variations in the antenna gain and beam-width. H_1 (Fig. 4(f)) was parametrically analyzed, in which its trends showed that as H_1 increased, the more stable the 3-dB beam width curves were for

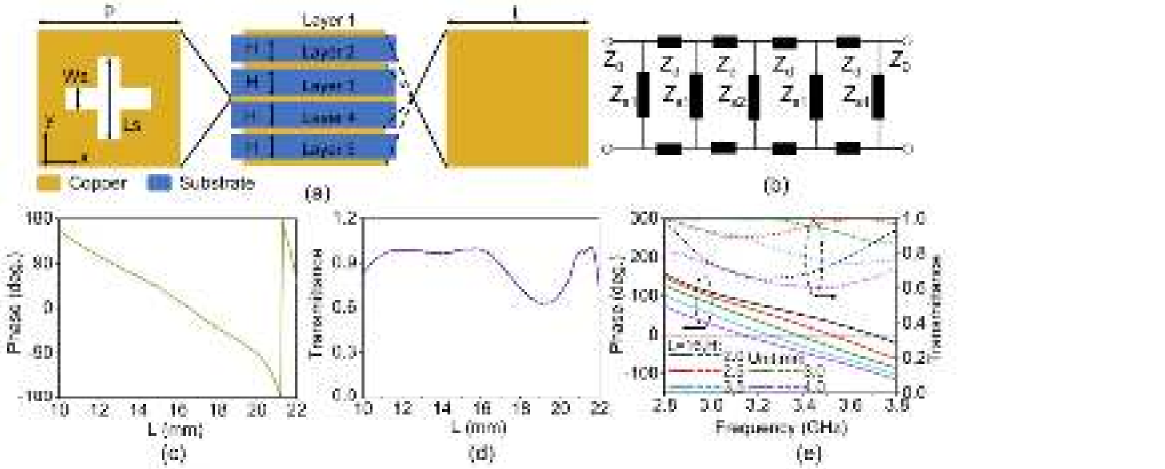

Fig. 6. (a) Geometry of the unit cell. (b) Equivalent TL model of the proposed meta lens unit cell. Phase (c) and magnitude (d) range of the transmission coefficient for varied L. (e) Simulated phase and magnitude of the transmission coefficient as a function of frequency with different values of H.

the E-plane at particular frequency bands of interest. However, its increases were followed by sharp decreases at higher frequencies. Therefore, 5 mm was selected as the optimal value to account for the effect of H_1 on the 3-dB beam width and gain.

A prototype was fabricated (Fig. 4(g)) to further verify the proposed antenna design. Here, the simulated and measured reflection coefficients of S_{11} were plotted in Fig. 4(g). It can be observed that S_{11} was less than −10 dB at the 2.95–3.82 GHz range, indicating the good impedance matching. The simulated and measured gains of the antenna are presented in Fig. 4(h). Using a well-designed AMC structure, the realized gain of the fabricated antenna over the operational frequency band reached approximately 8 dBi, while its corresponding radiation efficiency was found to be greater than 90%. Additionally, simulated cross and co-polarization levels of the antenna at different frequencies are presented in Fig. 4(i). A clear observation from Fig. 4(i) is that the cross-polarization gain is approximately 18 dB lower than the co-polarization gain within the radiation angles of interest (-30° ~ 30°) at three frequencies, which serves as a strong indicator of excellent linear polarization characteristics. Furthermore, the measured two-dimensional (2D) radiation patterns of the proposed antenna with AMC at 3.0 GHz, 3.3 GHz, and 3.6 GHz were also given in Fig. 5, in which the 3-dB beam width of the radiation patterns in E-plane and H-plane were approximately 60°, which was consistent with the simulated results (Fig. 5).

B. Meta-lens Design

A multilayer transmission-type meta-atom was adopted to compose the focusing lens (see Fig. 6(a)). This meta-atom exhibits a sandwich-shaped structure composed of square patches and cross slots, which were separated by dielectric substrates made of F4B with identical thickness H, permittivity of 2.65, and loss tangent of 0.001. The periodicity of meta-atom was 25 mm, having approximately 0.29λ at the working frequency of 3.3 GHz. The length and width of the cross slots were 15 mm and 3 mm, respectively. The basic unit cell of the meta-lens shown in Fig. 6(a) can be expressed as a TL model (Fig. 6(b)), in which its ABCD matrix can be derived as:

$$\begin{aligned}\begin{bmatrix} A & B \\ C & D \end{bmatrix} &= \begin{bmatrix} 1 & 0 \\ 1/Z_1 & 1 \end{bmatrix} \begin{bmatrix} \cos k_s H & jZ_s \sin k_s H \\ j\sin k_s H / Z_s & \cos k_s H \end{bmatrix} \\ &\quad \begin{bmatrix} 1 & 0 \\ 1/Z_1 & 1 \end{bmatrix} \begin{bmatrix} \cos k_s H & jZ_s \sin k_s H \\ j\sin k_s H / Z_s & \cos k_s H \end{bmatrix} \begin{bmatrix} 1 & 0 \\ 1/Z_2 & 1 \end{bmatrix} \\ &\quad \begin{bmatrix} \cos k_s H & jZ_s \sin k_s H \\ j\sin k_s H / Z_s & \cos k_s H \end{bmatrix} \begin{bmatrix} 1 & 0 \\ 1/Z_1 & 1 \end{bmatrix} \\ &\quad \begin{bmatrix} \cos k_s H & jZ_s \sin k_s H \\ j\sin k_s H / Z_s & \cos k_s H \end{bmatrix} \begin{bmatrix} 1 & 0 \\ 1/Z_1 & 1 \end{bmatrix}\end{aligned} \quad (3)$$

where Z_1 is the surface impedance of layer 1, layer 2, layer 4 and layer 5; Z_2 is the surface impedance of layer 3; and k_s is the propagation constant of the substrate. Based on Eq. (3), the transmission feature of the basic unit can be adjusted by modifying Z_1 and thickness H of the substrate once Z_2 has been determined. Owing to direct relationship of Z_2 with the structural parameter of the pattern, the transmission phase of the basic unit cell (at 3.3 GHz) can be fine-tuned to cover the 2π range, particularly as L varied from 10 mm to 22 mm (Fig. 6(c)). During this process, the basic unit cell exhibited relatively high transmission amplitudes (Fig. 6(d)), in which the transmission phase (solid lines) was shown in Fig. 6(e) as a function of the thickness of the substrate. The zero phase point that reflects the resonant frequency also gradually shifted to a lower frequency as H increased. When H was equal to 3.0 mm and 3.5 mm, the resonance that can motivate significant phase shifting occurred near 3.3 GHz. Finally, considering a better transmission coefficient, 3.0 mm was chosen as the optimum substrate thickness.

As shown in Fig. 6(c), the meta-atom exhibits a 360° phase modulation with high transmittance (Fig. 6(d)) when L in layers 1, 2, 4, and 5 varied from 10 mm to 22 mm. The meta-atom was employed based on its phase manipulating ability to construct a focusing lens according to the following equation:

$$T(x,y) = Ae^{jk_0(\sqrt{x^2+y^2+FL^2}-FL)} \quad (1)$$

where A is the amplitude value, which should have the maximum value in this design; FL is the predesigned focus

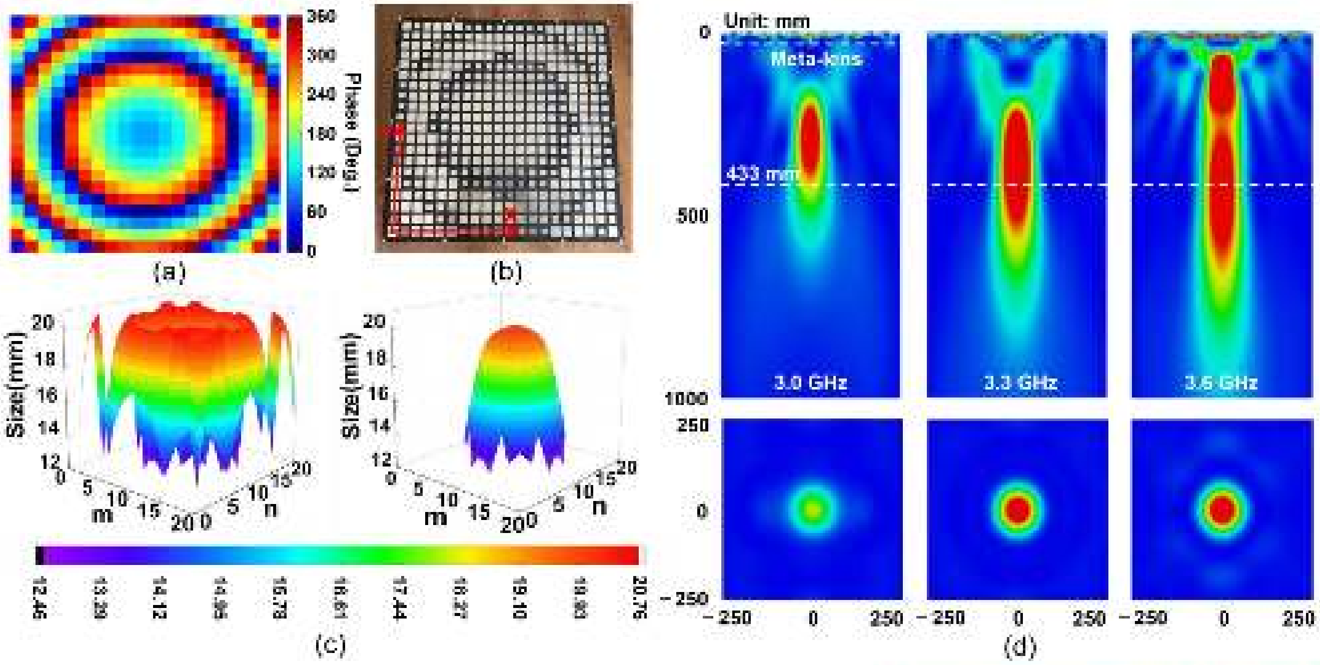

Fig. 7. (a) Phase distribution on the aperture at 3.3 GHz. (b) Fabricated broadband meta-lens. (c) Detailed L parameters of the meta-atoms at the aperture of the meta-lens. (d) Simulated focal performance of the meta-lens at 3.0 GHz, 3.3 GHz, and 3.6 GHz. (m denotes the m[th] unit along the x direction, and n denotes the n[th] unit along the y direction.)

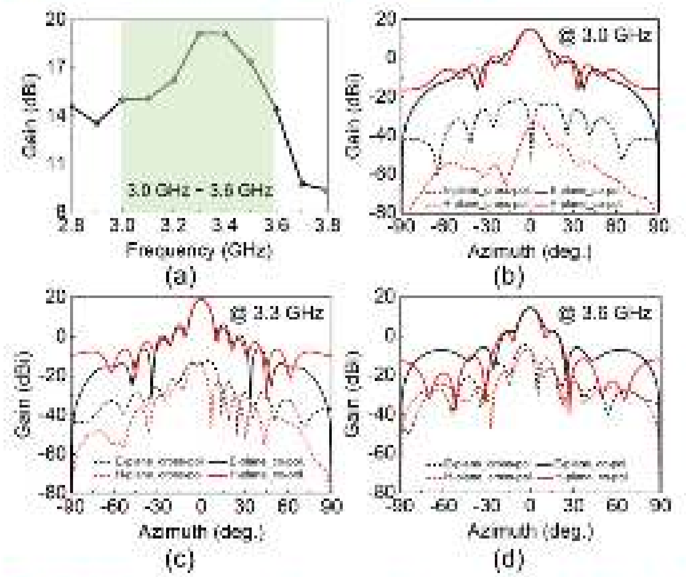

Fig. 8. (a) Simulated gain as a function of frequency. Simulated E-plane and H-plane radiation patterns of the proposed antenna with meta-lens at 3.0 GHz (b), 3.3 GHz (c), and 3.6 GHz (d).

length; and k is the wave number in free space. Here, (x, y) denotes the location of the basic meta-atoms across the meta-lens. Once the FL and coordinates (x, y) have been determined, the phase distribution at the aperture can be accurately derived using Eq. (4). However, owing to the close coupling between meta-atoms, the initial phase distribution obtained from Eq. (4) may not result in an optimal focal performance. To address this, Eq. (4) was modified to enhance the focal performance, given by Eq. (5):

$$I(x,y) = \Delta\varphi + Ae^{jk(\sqrt{x^2+y^2+FL^2}-FL)} \tag{5}$$

where $\Delta\varphi$ is a reference phase. Consequently, by comparing the presence of MAT situations (Fig. 10(a)), the varying S_{21} difference may be obtained as the $\Delta\varphi$ changes from 0° to 360°. Following multiple rounds of optimization, the $\Delta\varphi$ that is equal to 180° was selected to help obtain the S_{21} difference in the working bandwidth of >10 dB as shown in Fig. 10(c).

In this process, FL was calculated according to the basic design principle: the 3-dB beam width of the antenna ($\theta = 60°$) was approximately equal to the FOV (φ) of the meta-lens (Fig. 1(b)); thus, the relationship between the FL and side length (SL) of the meta-lens may be obtained by adopting the following equation:

$$SL / FL = 2\tan\frac{\varphi}{2}. \tag{6}$$

Considering the complexity of the array design, a meta-lens composed of 20 × 20 meta-atoms with an SL of 500 mm was formed. By substituting SL and $\varphi = 60°$ into Eq. (6), FL was calculated to be 433 mm. The corresponding phase distributions calculated using Eq. (5) is shown in Fig. 7(a). To meet the focusing performance at 3.0 GHz ~ 3.6 GHz, the focusing performance at 3.0 GHz, 3.3 GHz, and 3.6 GHz was investigated, as shown in Fig. 7(c). Although the focal length gradually increased with frequency, the compressed focal length at FL = 433 mm still has the potential to have a significantly enhanced power density. To investigate the impact of the meta-lens on the gain of the proposed antenna, we have plotted the simulated gain as a function of frequency in Fig. 8(a). It is evident that the antenna's gain experiences a significant enhancement with the presence of the meta-lens, surpassing the antenna's gain of 8 dBi without it and reaching an impressive 19 dBi.

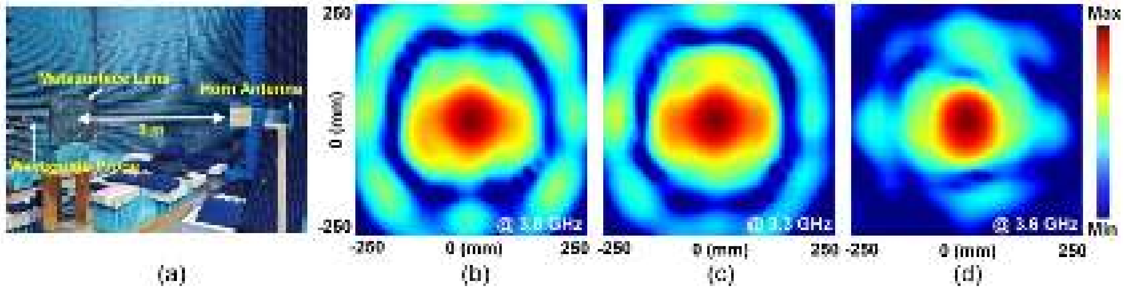

Fig. 9. (a) Photograph of the experimental setup. The measured focusing performance at (b) 3.0 GHz, (c) 3.3 GHz, and (d) 3.6 GHz.

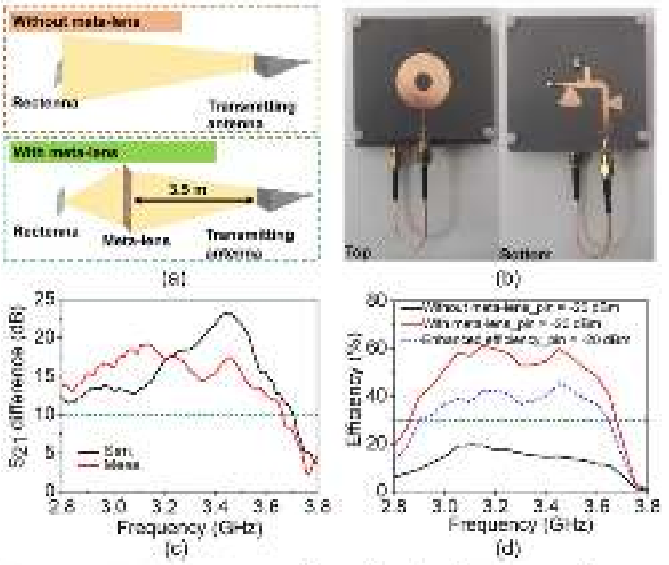

Fig. 10. (a) Measurement setup for evaluating the MAT performance. (b) Fabricated broadband rectenna. (c) Simulated and measured S_{21} difference from the transmitting antenna to the rectenna with and without MAT. (d) Measured efficiency of the rectenna with and without MAT as a function of frequency when the receiving power of the rectenna is preset as −20 dBm without meta-lens.

Furthermore, Figs. 8(b-d) showcase the E-plane and H-plane radiation patterns of the antenna equipped with the meta-lens at 3 GHz, 3.3 GHz, and 3.6 GHz. These visualizations clearly illustrate the generation of highly directional beams at these three frequencies, with sidelobe levels positioned 13 dB below the peak gain. Additionally, Figs. 8(b-d) provide a notable insight into the cross-polarization performance, showing that the cross-polarization gain is approximately 30 dB lower than the co-polarization gain. This low level of cross-polarization indicates excellent performance in this regard.

To further evaluate the performance of the proposed meta-lens, a sample was fabricated using the PCB technology based on the L-parameter variation in the (x, y) plane (Fig. 7(c)), as depicted in Fig. 7(b). The desired phase distribution was obtained by adjusting the L values of the square patches. Consequently, as shown in Fig. 7(b), the meta atoms spanning the aperture of the meta lens exhibit a gradient pattern. The prototype was consistent with the simulated model and was subsequently measured in an anechoic chamber. Here, near-field measurements were performed to detect the focusing effect. As shown in Fig. 9(a), the meta-lens was located on the platform and illuminated by the feed horn, and the near-field electric field distribution was detected by scanning the waveguide probe. The distance between the waveguide and prototype was equal to a focal length of 433 mm, and the scanning area was 500 mm × 500 mm. The normalized results in Figs. 9(b-d) illustrated a relatively acceptable focusing effect as the simulated prediction (Fig. 7(d)), which may serve as the basis for the next energy harvesting.

IV. Overall System Performance Measurement

Finally, to demonstrate the performance of the proposed RF-DC conversion system, two experiments were conducted to verify the enhanced performance of the meta-lens in terms of the receiving power and conversion efficiency of the rectenna. A commercial Vivaldi standard horn antenna and fabricated rectenna (Figs. 10(a-b)) were used as the transmitting and receiving antennas, respectively. First, the effect of the meta-lens on the receiving power of the receiving antenna was verified by connecting a two-port vector network analyzer to the transmitting and receiving antennas, in which S_{21} was measured with and without the meta-lens. Next, the receiving power enhancement provided by the meta-lens was evaluated by comparing S_{21} of the meta-lens-enhanced system with that of the system without the meta-lens. The S_{21} difference, which represents the receiving-power enhancement, was obtained by subtracting the two measurements. Fig. 10(c) shows the S_{21} difference obtained from both the simulation and measurement. Here, the meta-lens was positioned 433 mm from the fabricated rectenna, following the previous design specifications. Despite the variations attributed by the separate design approach, the measured S_{21} difference remained consistently >10 dB across the frequency range of 3.0 GHz to 3.6 GHz. This indicates a receiving-power increase of >10 dB, which was equivalent to a tenfold improvement, following the introduction of the meta-lens.

Meanwhile, the effect of the MAT on the total conversion efficiency was verified by connecting the transmitting antenna to a signal generator emitting RF energy, in which the receiving antenna was connected to a spectrum analyzer to identify the receiving power of the rectenna. By tuning the transmitting power, the receiving power can be fixed at −20 dBm, which mimics the ambient power level in typical cases. The antenna was then connected to the rectifier by a coaxial with the characteristic impedance of 50 Ω. Finally, the DC output current was measured using an amperometer, and the

TABLE III
COMPARISON OF THE PROPOSED RECTENNA AND RELATED DESIGN

Ref. (year)	Input Power: IBW (FBW)	Peak Conversion Efficiency (PCE) at −10 dBm	EB (FBW) at −10 dBm (Efficiency > 0.9*PCE)	EB (FBW) at −20 dBm (Efficiency > 40%)	Technique
[58] (2015)	−10 dBm: 1.77 GHz ~ 1.84 GHz (4%) 2.0 GHz ~ 2.24 GHz (10.3%)	56% @ 1.88 GHz	1.79 GHz ~1.92 GHz (7%) 2.06 GHz ~ 2.26 GHz (9%)	0%	Two-branch impedance matching technique
[43] (2020)	−3 dBm: 2.4 GHz ~ 2.6 GHz (8%) 2.18 GHz ~ 2.3 GHz (5%)	51% @ 1.8 GHz	NR	0%	Conjugate matching technique
[59] (2022)	−15 dBm: 2.25 GHz ~ 2.7 GHz (18%)	22% @ 2.4 GHz	NR	0%	Impedance matching technique
[11] (2019)	−10 dBm: 2.1 GHz ~ 2.5 GHz (17%)	37% @ 2.3 GHz	2.21 GHz ~2.4 GHz (8%)	0%	Impedance matching technique
This work (without meta-lens) (2023)	−10 dBm: 2.89 GHz ~ 3.7 GHz (24.5%) −20 dBm: 2.87 GHz ~ 3.7 GHz (25%)	47.1% @ 3.16 GHz	2.99 GHz ~ 3.6 GHz (18.5%)	0%	Impedance matching technique
This work (with meta-lens) (2023)	−10 dBm: 2.89 GHz ~ 3.7 GHz (24.5%) −20 dBm: 2.87 GHz ~ 3.7 GHz (25%)	63% @ 3.2 GHz	2.98 GHz ~ 3.65 GHz (20.2%)	2.90 GHz ~ 3.63 GHz (22.3%)	MAT

IBW: Impedance Bandwidth. EB: Efficiency Bandwidth. NR: Not Reported.

conversion efficiency without the meta-lens was calculated using Eq. (1). The meta-lens was then placed between the transmitting antenna and proposed rectenna (placed at the focal location). Without changing the emitting power, as in the above measurement, the receiving power and DC output current of the rectenna were measured and the efficiency of the meta-lens was calculated using the same method (Fig. 10(d)). It was demonstrated that the enhanced efficiency was more than 30% at 2.90 GHz ~ 3.63 GHz, with a maximum boost of 45%, indicating the proposed MAT have significant advantages in improving conversion efficiency of the rectenna at low RF power density.

A comparison between our rectenna design and related designs is presented in Table III. Here, not only did the fractional bandwidth (FBW) showed higher overall performance than those of the existing designs at an input power of −10 dBm, but also the corresponding efficiency of the proposed rectenna without the consideration of the MAT. Hence, it can be inferred that through the adoption of MAT, the efficiency of the total system may potentially reach >40% at 2.90 GHz ~ 3.63 GHz, which is already significantly higher than the that of state-of-the-art results for input power at approximately −20 dBm.

V. CONCLUSION

In this paper, we introduce a novel technique called the meta-lens-assisted technique (MAT) aimed at enhancing the conversion efficiency of broadband rectennas. MAT accomplishes this by amplifying the RF power density around the rectenna while leaving the working bandwidth unaffected. Notably, the MAT-empowered rectenna achieves an impressive RF-to-DC conversion efficiency exceeding 40% across a frequency range spanning from 2.90 GHz to 3.63 GHz, even when operating at low input power levels down to -20 dBm. In contrast, conventional designs typically exhibit efficiencies of less than 20% at such low power levels.

The potential of the MAT concept for practical implementation in real-world scenarios is substantial. It can be strategically integrated into various objects such as windows, furniture, and home appliances, serving as a passive amplifier and focusing medium. This capability opens the door to highly efficient wireless energy-harvesting systems. The design holds great promise for effective wireless energy harvesting, with applications in various aspects of daily life. Specifically, it offers significant advantages for powering IoT terminal devices, including wireless sensors, backscatters, RFIDs, digital clocks, smoke alarms, and DC-DC converters. Our proposed design facilitates efficient wireless energy harvesting, providing a novel approach to enhance low-power energy harvesting for IoT devices, especially when coupled with specific lens devices.

REFERENCES

[1] S. Shen, Y. Zhang, C. -Y. Chiu and R. Murch, "Directional multiport smbient RF rnergy-harvesting dystem for the internet of things," *IEEE Internet Things J.* vol. 8, no. 7, pp. 5850-5865, Apr. 2021.

[2] M. Wagih, G. S. Hilton, A. S. Weddell and S. Beeby, "Millimeter-wave power transmission for compact and large-area wearable IoT devices based on a higher order mode wearable antenna," *IEEE Internet Things J.*, vol. 9, no. 7, pp. 5229-5239, Apr. 2022.

[3] M. Kumar, S. Kumar, A. S. Bhadauria and A. Sharma, "A planar integrated rectenna array with 3-D-spherical DC coverage for orientation-tolerant wireless-power-transfer-enabled IoT sensor nodes," *IEEE Trans. Antennas and Propag.*, vol. 71, no. 2, pp. 1285-1294, Feb. 2023.

[4] X. Gu, L. Grauwin, D. Dousset, S. Hemour and K. Wu, "Dynamic ambient RF energy density measurements of montreal for battery-free IoT sensor network planning," *IEEE Internet Things J.*, vol. 8, no. 17, pp. 13209-13221, Sep. 2021.

[5] J. Kim and B. Clerckx, "Wireless information and power transfer for IoT: pulse position modulation, integrated receiver, and experimental validation," *IEEE Internet Things J.*, vol. 9, no. 14, pp. 12378-12394, Jul. 2022.

[6] G. Verma and V. Sharma, "A novel RF energy harvester for event-based environmental monitoring in wireless sensor networks," *IEEE Internet Things J.*, vol. 9, no. 5, pp. 3189-3203, Mar. 2022.

[7] Z. Liu, P. Wu and G. Li, "A multibeam and surface plasmonic clothing with RF energy-localized harvester for powering battery-free wireless sensor," *IEEE Internet Things J.*, vol. 9, no. 15, pp. 13955-13964, Aug. 2022.

[8] Q. Awais, Y. Jin, H. T. Chattha, M. Jamil, H. Qiang, and B. A. Khawaja, "A compact rectenna system with high conversion efficiency for wireless energy harvesting," *IEEE Access*, vol. 6, pp. 35857-35866, Jul. 2018.

[9] M. Pinuela, P. D. Mitcheson, and S. Lucyszyn, "Ambient RF energy harvesting in urban and semi-urban environments," *IEEE Trans. Microw. Theory and Techn.*, vol. 61, no. 7, pp. 2715-2726, Jul 2013.

[10] V. Marian, B. Allard, C. Vollaire, and J. Verdier, "Strategy for microwave energy harvesting from ambient field or a feeding source," *IEEE Trans. Power Electron.*, vol. 27, no. 11, pp. 4481-4491, Nov. 2012.

[11] Y. Shi, Y. Fan, Y. Li, L. Yang, and M. Wang, "An efficient broadband slotted rectenna for wireless power transfer at LTE band," *IEEE Trans. Antennas and Propag.*, vol. 67, no. 2, pp. 814-822, Feb. 2019.

[12] C. Song, Y. Huang, P. Carter, J. Zhou, S. D. Joseph, and G. Li, "Novel compact and broadband frequency-selectable rectennas for a wide input-power and load impedance range," *IEEE Trans. Antennas and Propag.*, vol. 66, no. 7, pp. 3306-3316, Apr. 2018.

[13] M. Kumar, S. Kumar, S. Jain and A. Sharma, "A plug-in type integrated rectenna cell for scalable RF battery using wireless energy harvesting system," *IEEE Microw. and Wireless Comp. Lett.*, vol. 33, no. 1, pp. 98-101, Jan. 2023

[14] S. Shen, C.-Y. Chiu, and R. D. Murch, "A dual-port triple-band L-probe microstrip patch rectenna for ambient RF energy harvesting," *IEEE Antennas and Wireless Propag. Lett.*, vol. 16, pp. 3071-3074, Oct. 2017.

[15] S. Chandravanshi, S. S. Sarma, and M. J. Akhtar, "Design of triple band differential rectenna for RF energy harvesting," *IEEE Trans. Antennas and Propag.*, vol. 66, no. 6, pp. 2716-2726, Jun. 2018.

[16] N. Mirzababaee, F. Geran, S. Mohanna, "A radio frequency energy harvesting rectenna for GSM, LTE, WLAN, and WiMAX," *RF and Microw.*, vol. 55, no. 2, pp. 35-42, Mar. 2021.

[17] X. Ruan and C. H. Chan, "An endfire circularly polarized complementary antenna array for 5G applications," *IEEE Trans. Antennas and Propag.*, vol. 68, no. 1, pp. 266-274, Jul. 2020.

[18] T. Li and Z. N. Chen, "Shared-surface dual-band antenna for 5G applications," *IEEE Trans. Antennas and Propag.*, vol. 68, no. 2, pp. 1128-1133, Feb. 2020.

[19] H. Sun, "An enhanced rectenna using differentially-fed rectifier for wireless power transmission," *IEEE Antennas and Wireless Propag. Lett.*, vol. 15, pp. 32-35, Apr. 2015.

[20] M. Zeng, A. S. Andrenko, X. Liu, Z. Li, and H.-Z. Tan, "A compact fractal loop rectenna for RF energy harvesting," *IEEE Antennas and Wireless Propag. Lett.*, vol. 16, pp. 2424-2427, Jul. 2017.

[21] K. Niotaki, S. Kim, S. Jeong, A. Collado, A. Georgiadis, and M. M. Tentzeris, "A compact dual-band rectenna using slot-loaded dual band folded dipole antenna," *IEEE Antennas and Wireless Propag. Lett.*, vol. 12, pp. 1634-1637, Dec. 2013.

[22] H. Tafekirt, J. Pelegri-Sebastia, A. Bouajaj, and B. M. Reda, "A sensitive triple-band rectifier for energy harvesting applications," *IEEE Access*, vol. 8, pp. 73659-73664, Apr. 2020.

[23] M. Wagih, A. S. Weddell, and S. Beeby, "Meshed high-impedance matching network-free rectenna optimized for additive manufacturing," *IEEE Open Journal of Antennas and Propag.*, vol. 1, pp. 615-626, Nov. 2020.

[24] H. Shen, Y. Guo, and Z. Zheng, "Design of a high-efficiency 2.45-GHz rectenna for low-input-power energy harvesting," *IEEE Antennas and Wireless Propag. Lett.*, vol. 11, pp. 929-932, Agu. 2012.

[25] H. Sun and W. Geyi, "A new rectenna using beamwidth-enhanced antenna array for RF power harvesting applications," *IEEE Antennas and Wireless Propag. Lett.*, vol. 16, pp. 1451-1454, Dec. 2016.

[26] S. M. Saeed, C. A. Balanis, C. R. Birtcher, A. C. Durgun, and H. N. Shaman, "Wearable flexible reconfigurable antenna integrated with artificial magnetic conductor," *IEEE Antennas and Wireless Propag. Lett.*, vol. 16, pp. 2396-2399, Jun. 2017.

[27] S. Chandravanshi, K. K. Katare, and M. J. Akhtar, "A flexible dual-band rectenna with full azimuth coverage," *IEEE Access*, vol. 9, pp. 27476-27484, Feb. 2021.

[28] S. Shen, Y. Zhang, C.-Y. Chiu, and R. Murch, "A triple-band high-Gain multibeam ambient RF energy harvesting system utilizing hybrid combining," *IEEE Trans. Indust. Electron.*, vol. 67, no. 11, pp. 9215-9226, Nov. 2020.

[29] H. Sun, H. He, and J. Huang, "Polarization-insensitive rectenna arrays with different power combining strategies," *IEEE Antennas and Wireless Propag. Lett.*, vol. 19, no. 3, pp. 492-496, Mar. 2020.

[30] L. Sun, Y. Li, and Z. Zhang, "Wideband decoupling of integrated slot antenna pairs for 5G smartphones," *IEEE Trans. Antennas and Propag.*, vol. 69, no. 4, pp. 2386-2391, Apr. 2021.

[31] K. Bhatt, S. Kumar, P. Kumar, and C. C. Tripathi, "Highly efficient 2.4 and 5.8 GHz dual-band rectenna for energy harvesting applications," *IEEE Antennas and Wireless Propag. Lett.*, vol. 18, no. 12, pp. 2637-2641, Dec. 2019.

[32] X. Li, L. Yang, and L. Huang, "Novel design of 2.45-GHz rectenna element and array for wireless power transmission," *IEEE Access*, vol. 7, pp. 28356-28362, Mar. 2019.

[33] C. Ding, H.-H. Sun, H. Zhu, and Y. Jay Guo, "Achieving wider bandwidth with full-wavelength dipoles for 5G base stations," *IEEE Trans. Antennas and Propag.*, vol. 68, no. 2, pp. 1119-1127, Feb. 2020.

[34] C. Song, Yi Huang, Paul Carter, and J Zhou, "A novel six-band dual cp rectenna using improved impedance matching technique for ambient RF energy harvesting," *IEEE Trans. Antennas and Propag.*, vol. 64, no. 7, pp. 3160-3171, Jul. 2016.

[35] Y. Wang et al., "Efficiency enhanced seven-band omnidirectional rectenna for RF energy harvesting," *IEEE Trans. Antennas and Propag.*, vol. 70, no. 9, pp. 8473-8484, Sep. 2022.

[36] C.-Y. Hsu, S.-C. Lin, and Z.-M. Tsai, "Quadband rectifier using resonant matching networks for enhanced harvesting capability," *IEEE Microw. and Wireless Comp. Lett.*, vol. 27, no. 7, pp. 669-671, Jul. 2017.

[37] H. Kim and S. Nam, "Performance enhancement of 5G millimeter wave antenna module integrated tablet device," *IEEE Trans. Antennas and Propag.*, vol. 69, no. 7, pp. 3800-3810, Jul. 2021.

[38] Y. Cheng and Y. Dong, "Wideband circularly polarized planar antenna array for 5G millimeter-wave applications," *IEEE Trans. Antennas and Propag.*, vol. 69, no. 5, pp. 2615-2627, May 2021.

[39] F. Xie, G.-M. Yang, and W. Geyi, "Optimal design of an antenna array for energy harvesting," *IEEE Antennas and Wireless Propag. Lett.*, vol. 12, pp. 155-158, Jan. 2013.

[40] H. Kanaya, S. Tsukamaoto, T. Hirabaru, D. Kanemoto, R. K. Pokharel, and K. Yoshida, "Energy harvesting circuit on a one-sided directional flexible antenna," *IEEE Microw. and Wireless Comp. Lett.*, vol. 23, no. 3, pp. 164-166, Mar. 2013.

[41] S. Shen, C.-Y. Chiu, and R. D. Murch, "Multiport pixel rectenna for ambient RF energy harvesting," *IEEE Trans. Antennas and Propag.*, vol. 66, no. 2, pp. 644-656, Feb. 2018.

[42] W. Liu, K. Huang, T. Wang, Z. Zhang, and J. Hou, "A broadband high-efficiency RF rectifier for ambient RF energy harvesting," *IEEE Microw. and Wireless Comp. Lett.*, vol. 30, no. 12, pp. 1185-1188, Dec. 2020.

[43] C. Song, P. Lu, and S. Shen, "Highly efficient omnidirectional integrated multiband wireless energy harvesters for compact sensor nodes of internet-of-things," *IEEE Trans. Indust. Electron.*, vol. 68, no. 9, pp. 8128-8140, Sep. 2021.

[44] T. N. Duong, J. Venkataraman and Z. Lu, "Enhancement of ambient energy harvesting using a metamaterial lens," in *IEEE Antennas and Propagation Society International Symposium*, Orlando (APSURSI), FL, USA, 2013, pp. 962-963.

[45] H. Sun and W. Geyi, "A new rectenna with all-polarization-receiving capability for wireless power transmission," *IEEE Antennas and Wireless Propag. Lett.*, vol. 15, pp. 814-817, Sep. 2016.

[46] Z. Ma and G. A. E. Vandenbosch, "Wideband harmonic rejection filtenna for wireless power transfer," *IEEE Trans. Antennas and Propag.*, vol. 62, no. 1, pp. 371-377, Jan. 2014.

[47] P. Lu, X.-S. Yang, J.-L. Li, and B.-Z. Wang, "Polarization reconfigurable broadband rectenna with tunable matching network for microwave power transmission," *IEEE Trans. Antennas and Propag.*, vol. 64, no. 3, pp. 1136-1141, Mar. 2016.

[48] Z. He and C. Liu, "A compact high-efficiency broadband rectifier with a wide dynamic range of input power for energy harvesting," *IEEE Microw. and Wireless Comp. Lett.*, vol. 30, no. 4, pp. 433-436, Apr. 2020.

[49] H. S. Park and S. K. Hong, "Broadband RF-to-DC rectifier with uncomplicated matching network," *IEEE Microw. and Wireless Comp. Lett.*, vol. 30, no. 1, pp. 43-46, Jan. 2020.

[50] C. Song et al., "Matching network elimination in broadband rectennas for high-efficiency wireless power transfer and energy harvesting," *IEEE Trans. Indust. Electron.*, vol. 64, no. 5, pp. 3950-3961, May 2017.

[51] "Skyworks SMS 7630-079lf," Nov. 2021. [Online]. Available: https://www.mouser.cn/datasheet/2/472/skyworks_surface_mount_schottky_diodes_200041w-1213983.pdf.

[52] Y. Guo, X. Ma, M. Pu, "High-efficiency and wide-angle beam steering based on catenary optical fields in ultrathin metalens," *Advanced Optical Materials*, vol. 6, pp. 2195-1071, Apr. 2018.

[53] O. Zetterstrom, N. J. G. Fonseca and O. Quevedo-Teruel, "Additively manufactured half-gutman lens antenna for mobile satellite communications," *IEEE Antennas and Wireless Propag. Lett.*, vol. 22, no. 4, pp. 759-763, Apr. 2023.

[54] P. Castillo-Tapia et al., "Two-dimensional beam steering using a stacked modulated geodesic luneburg lens array antenna for 5G and beyond," *IEEE Trans. Antennas and Propag.*, vol. 71, no. 1, pp. 487-496, Jan. 2023.

[55] O. Orgeira, G. León, N. J. G. Fonseca, P. Mongelos and O. Quevedo-Teruel, "Near-field focusing multibeam geodesic lens antenna for stable aggregate gain in far-field," *IEEE Trans. Antennas and Propag.*, vol. 70, no. 5, pp. 3320-3328, May 2022.

[56] L. Wang, Y. Chang, B. Li and P. Zhang, "Reconfigurable AMC structure based on multimode resonances," in *2019 IEEE MTT-S International Wireless Symposium (IWS)*, Guangzhou, China, 2019, pp. 1-3.

[57] S. M. Rouzegar, A. Alighanbari, and O. M. Ramahi, "Wideband uniplanar artificial magnetic conductors based on curved coupled microstrip line resonators," *IEEE Microw. and Wireless Comp. Lett.*, vol. 27, no. 4, pp. 326-328, Apr. 2017.

[58] C. Song, Y. Huang, J. Zhou, J. Zhang, S. Yuan, and P. Carter, "A high-efficiency broadband rectenna for ambient wireless energy harvesting," *IEEE Trans. Antennas and Propag.*, vol. 63, no. 8, pp. 3486-3495, Aug. 2015.

[59] S. F. Bo, J.-H. Ou, Y. Dong, S.-W. Dong, and X. Y. Zhang, "All-polarized wideband rectenna with enhanced efficiency within wide input power and load ranges," *IEEE Trans. Indust. Electron.*, vol. 69, no. 7, pp. 7470-7480, Jul. 2022.

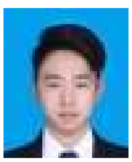

Yuchao Wang received the B.S. degree in electronic science and technology from the Wuhan University of Technology, Wuhan, China, in 2018, where he received the M.S. degree in 2021.

His research interests include planar antennas, RF energy harvesting, and wireless power transmission.

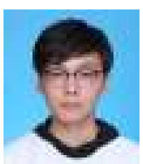

Shi He received the B.E degree in electronic and information engineering from Wuhan University of Technology, Wuhan, China, in 2016. He is currently pursuing the M.E degree in electronic and information engineering with Southeast University.

His current research interests include full-space metasurface and reconfigurable metasurface.

Yongxue Qiu received the B.E degree in polymer materials and engineering from Minjiang College, Fuzhou, China, in 2021. He is currently pursuing the M.E degree in materials science and engineering with Wuhan University of Technology.

His current research interests include full-space metasurface and reconfigurable metasurface.

Ruiyuan Wu received the B.Sc. degree from the school of electronic science and engineering, Nanjing University of Posts and Telecommunications, Nanjing, China, in 2014, and the Ph.D. degree with the school of information science and engineering, Southeast University (SEU), Nanjing, China, in 2020. He is currently a postdoctoral fellow with the state key laboratory of millimeter waves, SEU. His research interests include metasurface devices and systems, transmitarray and reflectarray antenna designs. He has authored or coauthored more than 30 publications, with citation over 1300 times.

Dr. Wu was a recipient of the best student paper award at the 11th UK-Europe-China workshop on millimeter waves and terahertz technologies (UCMMT) in 2018.

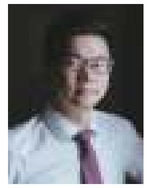

Lei Wang (Senior Member, IEEE) received the Ph.D. degree in electromagnetic field and microwave technology from the Southeast University, Nanjing, China in 2015. From November 2017 to February 2020, he was an Alexander von Humboldt scholar in the Institute of Electromagnetic Theory of Hamburg University of Technology (TUHH) in Hamburg, Germany. From March 2020 to present, he is an Assistant Professor in the Institute of Signals, Sensors and Systems of Heriot-Watt University in Edinburgh, United Kingdom. His research includes the antenna theory and applications, active electronically scanning arrays, integrated antennas and arrays, substrate-integrated waveguide antennas, leaky-wave antennas, and wireless propagations.

He was awarded the Chinese National Scholarship for PhD Candidates in 2014 and was granted the Swiss Government Excellence Scholarship to conduct research at EPFL in 2014 too. He was also granted by the Alexander von Humboldt Research Foundation to take research at TUHH in 2016. Moreover, he received the Best Poster Award in 2018 IEEE International Workshop on Antenna Technology (iWAT) and the Best Paper Award in the 5th International Conference on the UK-China Emerging Technologies (UCET2020).

Ping Lu (Member, IEEE) received the B.S. degree in electrical engineering and automation from Southwest Jiaotong University, Chengdu, China, in 2012, and the Ph.D. degree in radio physics from the University of Electronic Science and Technology, Chengdu, in 2018. From 2015 to 2017, she was a Joint Ph.D. Student Scholar with the Laboratoire Ampére, École Centrale de Lyon, INSA de Lyon, Université Claude Bernard de Lyon, Villeurbanne, France.

She is currently an Associate Professor with the School of Electronics and Information Engineering, Sichuan University, Chengdu. Her current research interests include rectenna, non-diffraction beams, and wireless power transmission.

Chaoyun Song (Senior Member, IEEE) received BEng. MSc and PhD degrees in electrical engineering and electronics from The University of Liverpool (UoL), Liverpool, UK, in 2012, 2013 and 2017, respectively.

He is currently an Associate Professor (Senior Lecturer) with the Department of Engineering, King's College London, London, UK. Prior to this, he was an Assistant Professor with the School of Engineering and Physical Sciences (EPS), Heriot-Watt University, Edinburgh, Scotland, UK. He has published more than 110 papers (including 45 IEEE transactions) in peer-reviewed journals and conference proceedings. His current research interests include wireless energy harvesting and power transfer, rectifying antennas (rectennas), flexible and stretchable electronics, metamaterials and meta-surface, and low-power sensors.

Dr. Song has been the recipient of numerous international awards, including the IEEE AP-S Young Professional Ambassador 2023, IEEE AP-S Raj Mittra Travel Grant 2023, EuCAP 2023 Best Antenna Paper Award, IET Innovation Award in 2018, and BAE Systems Chairman's Award in 2017. Additionally, Dr. Song has served as a session chair and/or TPC member for various conferences, including EuCAP2018, IEEE AP-S Symposium 2021, IEEE VTC2022-fall, EuCAP2023, IEEE AP-S Symposium 2023 and EuCAP2024. He has consistently contributed as a reviewer for esteemed journals such as Nature Electronics, Nature Communications, Advanced Materials, Advanced Functional Materials, and Nano Energy, in addition to reviewing for over fifteen IEEE Transactions. He is a Top-200 reviewer for IEEE Transactions on Antenna and Propagation (2021-2023). Dr. Song has also taken on the role of Guest Editor for prestigious publications including IEEE Open Journal on Antennas and Propagation, IET Electronic Letters, Micromachines, and Wireless Communications and Mobile Computing and an Associate Editor for Frontiers in Communications and Networks.

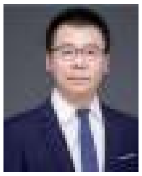

Qiang Cheng (M'15) received the B.S. and M.S. degrees from the Nanjing University of Aeronautics and Astronautics, Nanjing, Jiangsu, China, in 2001 and 2004, respectively, and the Ph.D. degree from Southeast University, Nanjing, in 2008.

In 2008, he joined the State Key Laboratory of Millimeter Waves, Southeast University, where he was involved in the development of metamaterials and metadevices. He is currently a Full Professor with the Radio Department, Southeast University. He leads a group of Ph.D. students and master students in the area of metamaterials, tunable microwaves circuits, microwave imaging, and terahertz systems. He has authored or co-authored more than one hundred publications, with citation over 2000 times.

Dr. Cheng was a recipient of the 2010 Best Paper Award from the New Journal of Physics, the Chinas Top Ten Scientific Advances of 2010, and the Second Class National Natural Science Award in 2014. He served as the Vice Chair for the 2008 and 2010 International Workshop on Metamaterials, Nanjing, China.

Cheng Zhang was born in Henan, China. He received the M.S. degree in material science and technology from Wuhan University of Technology, Wuhan, China, in 2015, and the Ph.D degree at the State Key Laboratory of Millimeter Waves, Department of Radio Engineering, Southeast University, Nanjing, in 2019. He is currently a Professor in Shanghai Institute of Optics and Fine Mechanics, Chinese Academy of Sciences, Shanghai 201800, China. His current research interests are EM energy harvesting, stealth metamaterial/metasurface and multi-physical manipulation. He has authored or co-authored more than fifty publications (including six highly cited papers), with citation over 1500 times.

He was a recipient of the 2020 CHINA TOP CITED PAPER AWARD from IOP Publishing and Top Articles in Device Physics for Applied Physics Letters (two papers). He received the Honor mention award for best student paper contest in 2018 IEEE International Workshop on Antenna Technology (iWAT) and the Appreciation award of invited talk in 2018 IEEE International Conference on Computational Electromagnetics (ICCEM).